Investigation of Water Evaporation Process at Air/Water Interface using Hofmeister Ions

Investigation of Water Evaporation Process at Air/Water Interface using Hofmeister Ions

Bhawna Rana[†], David J. Fairhurst[‡], and Kailash C. Jena*[,†,ǂ]

[†]Department of Physics and [ǂ]Department of Biomedical Engineering, Indian Institute of Technology Ropar, Rupnagar, Punjab-140001, India

[‡]Department of Physics and Mathematics, School of Science and Technology, Nottingham Trent University, Nottingham, Clifton Campus, NG11 8NS, United Kingdom

KEYWORDS (Water, Evaporation, Interface, sum frequency generation, Hofmeister Ions, H-bonding, Free OH).

ABSTRACT: Evaporation is an interfacial phenomenon in which a water molecule breaks the intermolecular hydrogen (H-) bonds with its associates and enters the vapor phase. However, a detailed demonstration of the role of interfacial water structure in the evaporation process is still ambiguous. Here, we purposefully perturb the H-bonding environment at the air/water interface by introducing kosmotropic (HPO_4^{-2}, SO_4^{-2}, and CO_3^{-2}) and chaotropic ions (NO_3^- and I^-) to excerpt their influence on the evaporation process. Using time-resolved interferometry on aqueous salt-droplets, we found that kosmotropes reduce evaporation, whereas chaotropes accelerate the evaporation process that follows the Hofmeister series $HPO_4^{-2} < SO_4^{-2} < CO_3^{-2} < Cl^- < NO_3^- < I^-$. In order to extract deeper molecular level insights about the observed Hofmeister trend in the evaporation rates, we investigated the air/water interface in presence of ions using surface-specific sum frequency generation (SFG) vibrational spectroscopy. The SFG vibrational spectra reveal the significant impact of ions on the strength of the H-bonding environment and the orientation of free OH oscillators from ~ 36.2º to 48.4º at the air/water interface, where both the variations follow the Hofmeister series. It is established that the slow evaporating water molecules experiencing a strong H-bonding environment with the free OH oscillators tilted away from the surface normal in the presence of kosmotropes at the air/aqueous interface. In contrast, the fast evaporating water molecules experienced a weak H-bonding environment with free OH oscillators tilted towards the surface normal in the presence of chaotropes at the air/aqueous interface. Our experimental outcomes showcase the complex bonding environment of interfacial water molecules and their decisive role in evaporation at the air/water interface.

INTRODUCTION

Understanding and controlling water evaporation is of great importance in diverse fields of science and technology, including surface patterning, optical mapping of DNA molecules, biological activity on Mars, separating crude oil from water, water harvesting, and disease diagnosis in pharmaceutical industries, etc.[1-6] In the domain of environmental sciences, the rate of evaporation of water molecules from the surface of aqueous aerosols decides the formation or growth of cloud droplets, which plays an indispensable role in maintaining the earth's water cycle and global temperature.[7-9] Thus, understanding water evaporation is of general interest. Despite the prevailing importance of evaporation in our daily lives, the molecular-level understanding of this phenomenon is still speculative. The water molecule breaks its hydrogen bonds (H-bonds) with neighboring molecules and leaves the interface to enter the air during the evaporation process. It is worth emphasizing that the interfacial molecular structure of water is quite different from the bulk, displaying a constellation of mono-, di-, tri-, and tetra- coordinated water species, with dangling/free OH, weakly H-bonded, and strongly H-bonded water molecules.[10-11] Therefore, the H-bonding environment of the interfacial water molecules inherently carries the potential to play a vital role in the evaporation process.

Previous studies of the evaporation of water droplets have shown the influence of co-solvents, gravity, and magnetic fields on evaporation dynamics.[12-15] Recently, Li *et al.*[13] and Edwards *et al.*[15] observed that gravity reverses the convective flows within the evaporating binary micro-droplets. Furthermore, it is also demonstrated that the presence of a magnetic field affects the thermo-solutal advection and enhances the evaporation rates of paramagnetic aqueous droplets.[14] Evidently, these studies present an understanding of the evaporation phenomenon through macroscopic diffusion, thermal convection, and solutal advection. Molecular dynamics (MD) simulation studies have attempted to develop a molecular-level understanding of the process.[16-19] For example, Varillay *et al.* have shown that evaporation can be considered as a ballistic escape from the liquid surface where molecules in the higher energy tail of the Boltzmann's distribution are more susceptible to breaking free.[16] According to Mason, the water species having H-bond coordination number one and two possess sufficient energy to escape from the liquid surface.[17] Recently, Nagata *et al.* reported that exactly 44fs after an H-bond formation, two oscillating water molecules are at the closest ap-

proach, and provide a sufficiently strong energetic kick to a third molecule to get it ejected from the surface.[18] In addition, Musolino et al. proposed that the orientation of surface water molecules can also influence the evaporation kinetics.[19] The prevailing literature highlights the importance of how the detailed H-bonding environment and orientation of water molecules is required for a complete mechanistic depiction of the evaporation process. The contribution of free OH (dangling) groups that constitute more than 20% of the population at the topmost water layer of the air/water interface;[20] towards the evaporation process is not explored yet. This prompted us to offer a detailed experimental demonstration with quantitative analysis to reveal the role of interfacial water molecules and their bonding environment in the evaporation process.

In the present study, we build a comprehensive understanding of the evaporation phenomenon by probing the conformation and H-bonding environment of water molecules at the air/aqueous interface. The H-bonded network can be easily perturbed in the presence of guest moieties.[10-11, 21-24] We have used this fact and purposefully employed a series of Hofmeister sodium salts; the selected anions are as follows:

$$HPO_4^{-2} > SO_4^{-2} > CO_3^{-2} > Cl^- > NO_3^- > I^- \qquad (1)$$

Franz Hofmeister reported this series in 1888 in which ions are placed as per their capacity to precipitate proteins from their aqueous solution.[25] The ions to the left of chloride ion are known as kosmotropes (structure-makers) while those to the right as chaotropes (structure-breakers).[25-31] The ions have a significant structuring effect on the bonding environment of water molecules at the air/aqueous interface. Therefore, we have selectively utilized the influence of Hofmeister ions to tune the interfacial structure of water molecules to extract new molecular-level insights about the evaporation process.

Here, we first studied the impact of Hofmeister ions on evaporation dynamics of sessile water droplets using an in-house time-resolved interferometry setup. It is observed that the kosmotropes impede evaporation, whereas chaotropes accelerate the evaporation rate compared to the pristine air/water interface. The observed ion-specific variation in the evaporation rates is ascribed to the variation in interfacial water structure at the air/aqueous interface as investigated by Sum frequency generation (SFG) vibrational spectroscopy. We have performed orientation angle calculation for free OH oscillator at air/aqueous interface in the presence of ions to see their influence on evaporation. It is found that the kosmotropes promote strongly H-bonded water species at the interface with free OH oscillators tilted away from the surface normal reflects the signature of slowing down the evaporation process. In contrast, the presence of chaotropes brings weakly bonded water species with free OH oscillator tilted more towards the surface normal, accelerating the evaporation.

EXPERIMENTAL SECTION

Materials

In the present work, we have performed experiments with six inorganic sodium salts (Na_2HPO_4, Na_2SO_4, Na_2CO_3, NaCl, $NaNO_3$, and NaI), purchased from Sigma Aldrich and used without any further purification.

Time-Resolved Interferometry

Figure 1a presents the experimental setup of time-resolved interferometry used to estimate the evaporation rate of sessile droplets. In this setup, a low-power He-Ne laser beam (λ = 543 nm) is directed onto the surface of a droplet sitting on a glass prism of refractive index 1.5.

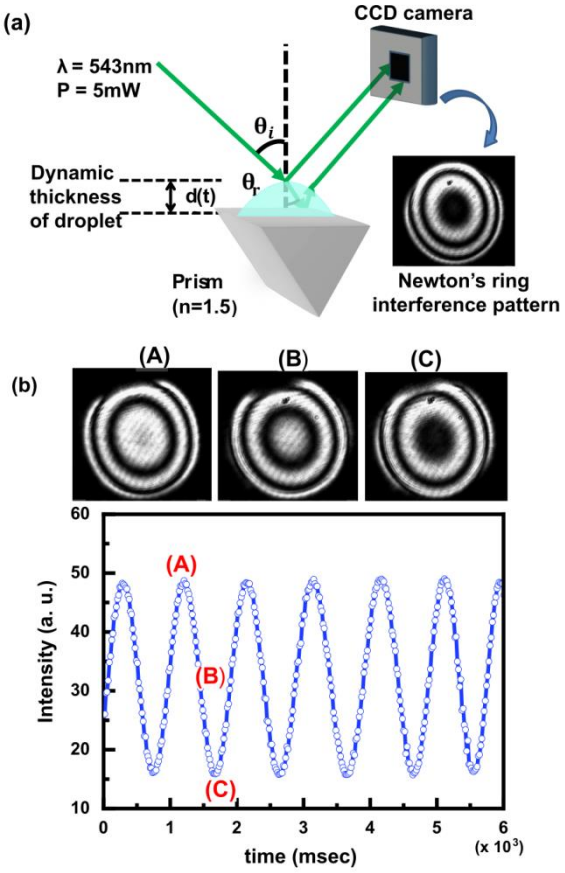

Figure 1. (a) Schematic of time-resolved interferometry for the evaporation rate studies of sessile aqueous droplets. (b) The snapshots with the intensity of the central fringe of the dynamic Newton's ring pattern with the time sequence of one fringe collapse (marked as A, B, and C, respectively).

The Fresnel reflections generated from the top and bottom surfaces form a Newton's ring interference pattern. The intensity of the interference pattern was recorded using a CCD camera for subsequent analysis. As the droplet is continuously evaporating, the droplet's moving surface, of height (d) leads to a dynamic optical path and consequently a varying phase difference between the interfering beams, which is given by:[32]

$$\Delta\phi(t) = \frac{2\pi}{\lambda}\left(\frac{2n_l d(t)}{\cos\theta_r}\right) \qquad (2)$$

Here, n_l is the refractive index of the liquid medium and θ_r (~8°) the angle of refraction. The intensity of the central fringe pattern as a function of time is given by:[32]

$$I(t) \propto \cos^2(\Delta\phi(t)) \quad (3)$$

The variation in the intensity of the central fringe of dynamic Newton's ring interference pattern is shown in figure 1b, with snapshots at various stages of one fringe collapse are designated by A, B, and C, respectively. The variable intensity profile is then utilized to calculate the change in droplet height $\Delta d(t)$ as follows. The variation in the central fringe intensity from one maximum (or minimum) to the next, results in a phase change of $\Delta\phi = 2\pi$, thus moving over (k+1) maxima gives a change in droplet thickness as given by:

$$\Delta d(t) = k\left(\frac{\lambda \cos\theta_r}{2n_l}\right) \quad (4)$$

Here, k is an integer having values 0, 1, 2, 3 etc. Plotting $\Delta d(t)$ with time gives a straight line plot, the slope of which measures the evaporation rate. In the present experiments, we have performed evaporation rate studies with 20 µl aqueous sessile droplets of pristine water and 1M sodium salt solutions. All the solutions are prepared in deionized water (Merck, Millipore direct-Q3, electrical resistivity of 18 MΩ.cm).

Sum Frequency Generation Vibrational Spectroscopy

In the present study, we have used an SFG Spectrometer (EKSPLA, Lithuania, SFG061) consisting of a mode-locked Nd:YAG picosecond diode pumped solid state (DPSS) laser system (PL2231-50), which provides a 30ps infrared (IR) beam at 1064 nm with output energy 40mJ at a repetition rate of 50 Hz. This fundamental beam is then used in the second harmonic generation unit (SFGH500-2H) to generate the visible beam at 532 nm. The fundamental (1064 nm) and the second harmonic (532 nm) beams then fed to the optical parametric generation unit (PG501-DFG2) that generates the tunable IR from 2300 nm to 16000 nm in the output. This visible 532 nm (diameter ~200 µm with 500 µJ energy/pulse) and tunable IR (diameter ~150 µm with 235 µJ energy/pulse at 3000 nm) were incident on the sample surface at angles around 63° and 56°, respectively with respect to the surface normal. The resultant sum frequency signal reflected at an angle of 61° is then allowed to pass through the detection optics. The intensity of the SFG signal is given as: [28-29, 33-40]

$$I \propto \left|\chi^{(2),eff}\right|^2 I_1 I_2 \quad (5)$$

Here, I_1 and I_2 are the intensities of visible and IR beams. $\chi^{(2),eff}$ is a second-order nonlinear susceptibility tensor, can be expressed as:

$$\chi^{(2),eff} = \chi^{(2)}_{NR} + \sum_v \frac{A_v}{(\omega_v - \omega_2 - i\Gamma_v)} \quad (6)$$

Here, $\chi^{(2)}_{NR}$ is the non-resonant component of the susceptibility, and the second term is the resonant part represented by a Lorentzian function. Resonance occurs when ω_2 (IR frequency) matches with the vibrational characteristic frequency (ω_v) of the molecules present at the interface. Here, A_v and Γ_v is the amplitude and the half-width at half maxima (HWHM) of the Lorentzian line shape, respectively. All the SFG spectra are collected in different polarization schemes (ssp and ppp) in the OH stretching region from 2800 to 3800 cm^{-1} at a step size of 2 cm^{-1} and acquisition per step of 200 and are fitted with Lorentzian line shape using equations (5-6). All the aqueous samples for SFG measurements are prepared in deionized water. We used a Teflon sample cell (diameter ~5cm) to carry the aqueous sample for SFG measurements. The sample cell is cleaned every time before the experiment using a piranha solution (3:1 v/v of concentrated sulphuric acid to 30% hydrogen peroxide solution) and then rinsed thoroughly with deionized water. All the experiments are conducted in the lab temperature of 21.5±0.5ºC.

RESULTS AND DISCUSSION

Figure 2a shows plots of change in central thickness $\Delta d(t)$ vs. t for aqueous droplets of pristine water and that of different sodium salt solutions with initial concentration of 1M. The slopes of these plots are utilized to quantify the evaporation rate values. The ion-specific evaporation rates of sessile droplets (figure 2b) follow the Hofmeister series as follows:

$$HPO_4^{-2} < SO_4^{-2} < CO_3^{-2} < Cl^- < NO_3^- < I^- \quad (7)$$

with a minimum evaporation rate for Na_2HPO_4 (83 nm/sec) and a maximum evaporation rate for NaI (333 nm/sec).

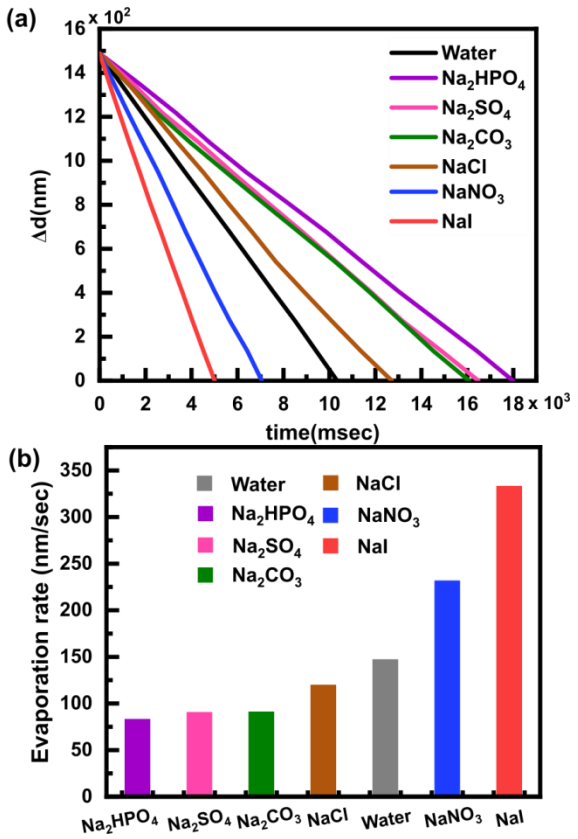

Figure 2. (a) Change in droplet central thickness (Δd) vs. time for sessile aqueous droplets of pristine water and 1M sodium salt solutions. The slopes of these experimental plots provide evaporation rates at the air/aqueous interface (panel (b).

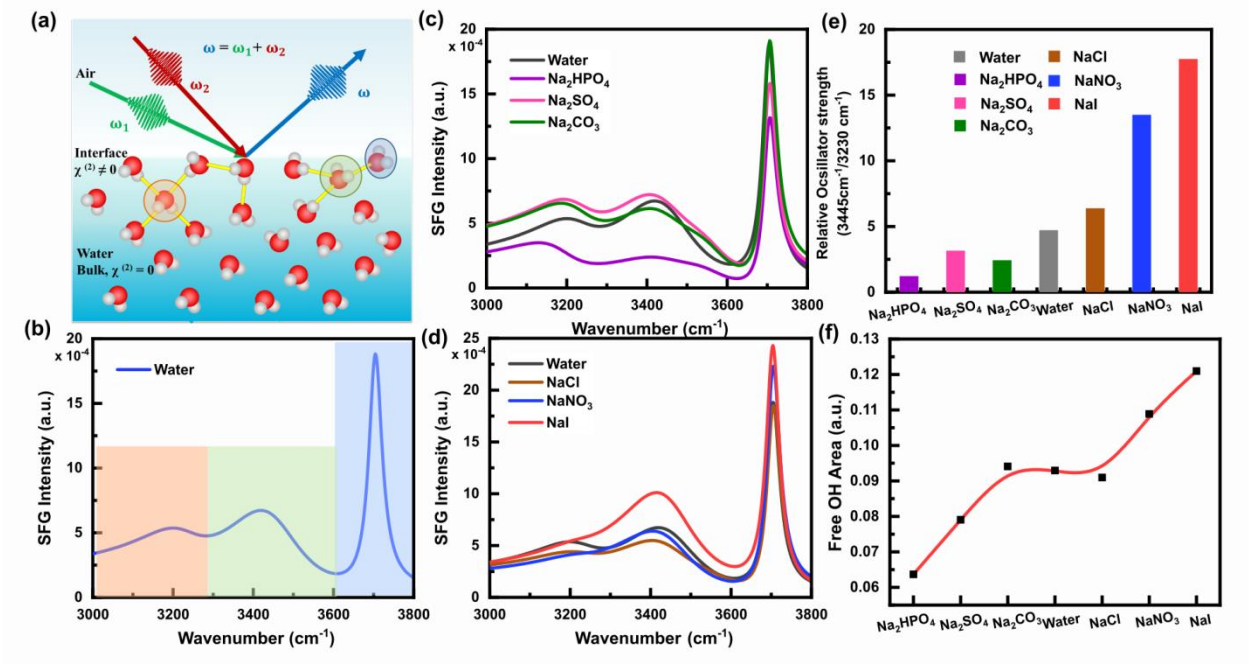

Figure 3. (a) Sketch of SFG vibrational spectroscopic experiments on air/aqueous interface. (b) SFG spectrum collected from pristine air/water interface in ssp polarization scheme; water species contributing into the shaded region of the spectrum are presented in panel (a). Polarization scheme ssp designates s-SFG, s-visible, and p-polarization of IR beams. Panel (c) and (d) SFG spectra at air/aqueous interface in the presence of 1M Hofmeister series sodium salts. The curves are Lorentzian fitted profiles; the fitting parameters are provided in table S2. Panel (e) and (f) represent the variation in relative oscillator strength (amplitude ratio of SFG peaks at 3445 cm^{-1} and 3230 cm^{-1}) and the integrated area under the free OH peak (3660 cm^{-1} to 3750 cm^{-1}) as a function of ions at the air/aqueous interface.

Evidently, the presence of kosmotropes (HPO_4^{-2}, SO_4^{-2}, and CO_3^{-2}) impedes the evaporation, whereas the presence of chaotropes (NO_3^- and I^-) accelerate the evaporation rate at the air/aqueous interface compared to the pristine water droplet (147 nm/sec). We have also carried out salt concentration-dependent evaporation rate studies on aqueous sessile droplets. The results are shown in section S2-I of supporting infromation. The evaporation rate decreases with the increase in the salt concentration, and the overall trend for various salts follows the similar Hofmeister series. The findings from the time-resolved interferometry experiment confirm the significant impact of ions on the evaporation process.

To extract a detailed molecular-level understanding of the observed Hofmeister trend in the evaporation rate, we have employed SFG vibrational spectroscopy to probe the influence of ions on interfacial water structure at the air/aqueous interface. The schematic layout of the SFG experiments is presented in figure 3a. SFG vibrational spectroscopy is an ideal spectroscopic tool to selectively probe the conformation and structure of the moieties lie in the interfacial region and is based on second-order nonlinear optical process.[28-29, 33-40] We consider the SFG spectrum at the pristine air/water interface as the reference spectrum to observe the comparative impact of various salts (Figure 3b). The spectra (Figure 3b-d) consist of a broad region from 3000 to 3650 cm^{-1} is assigned with three peak positions at around 3230, 3445, and 3550 cm^{-1}. The lowest frequency ensemble is attributed to strongly H-bonded (tetrahedral coordinated) water molecules, and the higher frequency peaks correspond to weakly H-bonded water molecules, however, still the exact assignment of these peaks continues to be ambiguous.[23,28,33,38-42] The sharp peak at 3704 cm^{-1} corresponds to the stretching mode of non-hydrogen bonded free OH oscillator (dangling bond) of water molecules protruding out of the interface. The SFG intensity plots shown in figure 3 (c and d) reflect the water spectra in the presence of ions at the air/aqueous interface.[28-29] For our analysis, we have considered the peak amplitude ratio of 3445 cm^{-1} to 3230 cm^{-1} to estimate the strength of the H-bonding environment of water molecules present at the interface.[39, 41] It is quite evident from the SFG plots that the presence of ions significantly perturbs the H-bonding environment of the water molecules. The relative enhancement in SFG intensity around 3230 cm^{-1} in the presence of kosmotropes ($HPO_4^{-2}, SO_4^{-2}, CO_3^{-2}$) and at 3445 cm^{-1} for chaotropes (NO_3^- and I^-) has been attributed to the size, charge, polarizability, and surface propensity of respective ions at the air/aqueous interface.[28-29] We have plotted the variation in relative oscillator strength as a function of ions present at the interface (figure 3e). The relative oscillator strength follows the Hofmeister series (equation 7), where the minimum value is observed for HPO_4^{-2}, and maximum in the presence of I^-. It indicates the ability of kosmotropes to make more strongly H-bonded water species at the interface compared to the neat air/water interface. In contrast, we have witnessed an increase in the weakly H-bonded molecules in the presence of chaotropes.

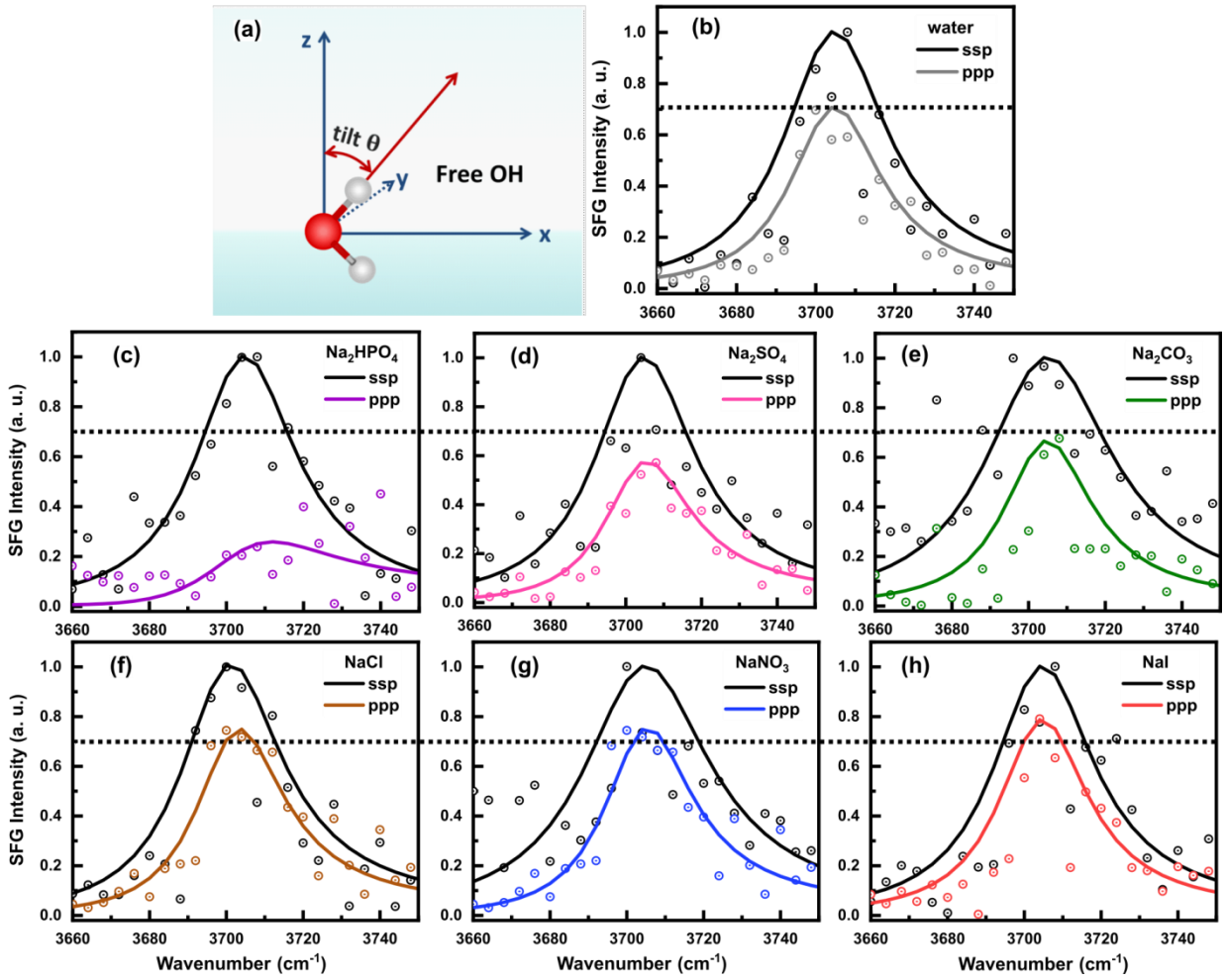

Figure 4. (a) Representation of orientation angle (tilt angle) θ formed by free OH oscillator with the surface normal. (b)-(h) SFG intensity spectra for free OH oscillator at air/aqueous interface in the presence of various 1M Hofmeister series sodium salts in ssp and ppp-polarization schemes. The points show experimental data, and the solid lines are the Lorentzian fit curves. Fitting parameters are given in table S3 of the supporting information. The horizontal dotted line reflects the aparent ion-specific variation in ppp-spectral intensity of free OH peak compared to pristine air/water interface (b).

Figure 3f demonstrates the variation in free OH peak area as a function of various ions. An increasing trend is observed moving from kosmotropes towards chaotropes, with minimum free OH area for Na_2HPO_4 and a maximum value for NaI. This observation can be attributed to the possible enhanced population of free OH water molecules in the presence of chaotropes compared to kosmotropes at the interfacial region. This is because the SFG signal intensity is proportional to $N_S < \cos\theta >$. Here, N_S represents the number of molecules participating in the SFG process at the interface while θ is the orientation angle.[20, 33] Therefore, the contribution from θ cannot be ignored; for which, we must consider the contribution of the orientation of free OH oscillators towards the observed variation in the SFG intensity or integrated area.

We performed a quantitative analysis to determine the impact of Hofmeister ions on the orientation of free OH groups at the air/aqueous interface. Du *et al.*[20] first studied the orientation of free OH groups at the air/aqueous interface and this was subsequently investigated by various groups.[43-46] Figure 4 shows the recorded SFG spectra in ssp and ppp-polarization schemes at the air/aqueous interface in the presence of 1M sodium salts from 3660 cm^{-1} to 3750 cm^{-1}. For our analysis, we have normalized the ssp-SFG spectra and accordingly scaled the ppp-SFG spectra; which demonstrate the ion-specific perturbations in the free OH peak intensity. The free OH spectral profiles recorded in ssp and ppp-schemes are then utilized for the calculation of orientation angle of free OH oscillator with respect to the surface normal (figure 5a). The detailed theory and calculation of the orientation angle of free OH are discussed in sections S1 and S2-II of the supporting information.

For the pristine air/water interface, we determine the free OH angle to be 37.6° which is in close agreement with the values reported in the literature.[20,44,46-47] In comparison to the pristine air/water interface, we have observed an enhancement in free OH tilt angle in the presence of kosmotropes, whereas a minute decrement is observed for chaotropes. Figure 5a (left axis) shows the variation in orientation angle of free OH as a

function of ions present at the air/aqueous interface, which follows the Hofmeister series (equation1):

$$HPO_4^{-2} > SO_4^{-2} > CO_3^{-2} > Cl^- > NO_3^- > I^-$$

The free OH orientation angle is maximum ~ 48.4° in the presence of Na_2HPO_4, and decreases as we move from kosmotropes to chaotropes (left to right, figure 5a) with a minimum value of 36.2° in the presence of NaI. In the past, ion-specific orientation studies of free OH groups have not been explored in detail. A recent report by Feng *et al.* showed that the presence of NaF (kosmotrope) rotates the free OH group away from the surface normal.[47] This finding is in good agreement with our experimental observations of reorientation of free OH oscillator towards the air/aqueous interface in the presence of kosmotropic ions. The significant increase in free OH tilt angle in the presence of HPO_4^{-2} and SO_4^{-2} correlates well with the previously observed decrease in free OH peak area (figure

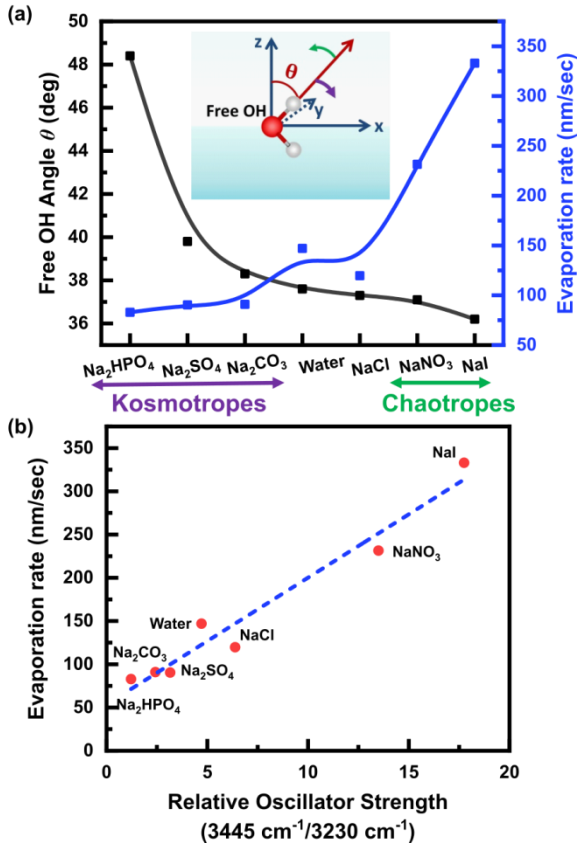

Figure 5. (a) Ion-specific variation in tilt angle values of free OH oscillator (left axis) in inverse correlation with the evaporation rates (right axis) studied at the air/aqueous interface. (b) Evaporation rates of the sessile droplets obtained from interferometry experiment (figure 2b) plotted as a function of relative OH oscillator strength observed from SFG spectra (figure 3c-d).

3f). However, for the case of chaotropes, the relative change in the orientation of the free OH group is quite small and is tilted more towards the surface normal. This indicates that the increase in the SFG signal for chaotropes (figure 3f) might have arisen due to an increase in the population of free OH groups at the interfacial region.

The right axis of figure 5a represents the ion-specific evaporation rates at the air/aqueous interface, which are found to follow an inverse correlation with the observed trend of free OH tilt angle in the presence of ions. Moreover, figure 5b provides a linear and direct correlation between the sessile droplet's evaporation rates (figure 2b) against the relative oscillator strength acquired from SFG spectra (figure 3e). Combining the observations from figure 5, we can conclude that the presence of kosmotropes (HPO_4^{-2}, SO_4^{-2}, and CO_3^{-2}) brings more strongly H-bonded water moieties at the air/aqueous interface, with free OH oscillators significantly tilted away from the surface normal. This, in turn, lowers the evaporation rates compared to the pristine air/water interface. However, with chaotropes (NO_3^- and I^-), we find a more weakly H-bonded environment with a little reorientation of free OH oscillators towards the surface normal, resulting in a higher evaporation rate.

The impact of the strength of the H-bonding environment and orientation of the free OH oscillator on the evaporation process can be understood as follows: A water molecule possesses 9-degrees of freedom; 3-translational, 3-rotational, and 3-vibrational.[16-17,19] When a water molecule binds to other molecules, it loses degrees of freedom resulting in a reduction in its average energy. In addition, the orientation of water OH oscillator plays an essential role in the formation of H-bonds[46-48] and hence, in turn, determines the average energy of surface water molecules. This is quite consistent with the reported molecular dynamics study, where Musolino *et al.* reported that the water molecule with dipole vector oriented more towards the surface normal loses its H-bonds with nearest neighbors and carries high average energies at the air/water interface.[19] In addition, the average energy difference between tetrahedral and monomer configuration of interfacial water molecule is found to be comparable with the enthalpy of vaporization that is 11.5kcal/mol.[19] This indicates that the strongly H-bonded species and the conformation of surface water molecules with free OH groups tilted away from the surface normal as observed in the presence of kosmotropes belong to the configuration of low average energy. This lower energy configuration must be responsible for slowing down the evaporation process. In distinction, the possible decrease in the H-bonding strength of surface water molecules with the presence of enhanced population of free OH oscillators possess high average energies, accelerate the evaporation process for chaotropes.

CONCLUSIONS

In summary, we have used surface-specific SFG vibrational spectroscopy and time-resolved interferometry to establish an intriguing correlation between the interfacial water structure (H-bonding and orientation of free OH oscillators) and the evaporation process. Structure making and breaking Hofmeister ions provided a platform to visualize the conformation of water molecules characteristic of slow/fast evaporation at the air/aqueous interface. Presence of kosmotropes (HPO_4^{-2}, SO_4^{-2}, and CO_3^{-2}) foster strongly H-bonded water molecules with an increase in the tilt angle of the free OH oscillators at the interface, slows down the evaporation. However, for the case of chaotropes (NO_3^- and I^-), we find a more weakly H-bonded

environment with little impact on the orientation of free OH oscillators, with possible enhanced population of free OH oscillators results in higher evaporation rate. These findings reveal a deeper fundamental insight into the prevailing concerns on evaporation. The outcomes of this work would help in designing interfacial water structures to manipulate the evaporation processes for future needs.

ASSOCIATED CONTENT

Supporting Information includes a detailed quantitative description for the calculation of orientation angle of free OH oscillator at the air/aqueous interface, Plots on variation in droplet central thickness vs. time showing impact of concentration of ions on evaporation of sessile aqueous droplets, tables of Lorentzian fitting parameters of SFG spectra in ssp and ppp-polarization schemes, table of orientation angle values of the free OH at the air/aqueous interface in the presence of ions. This material is available free of charge via the Internet at http://pubs.acs.org.

AUTHOR INFORMATION

Corresponding Author

* Kailash C. Jena- Department of Physics and Department of Biomedical Engineering, Indian Institute of Technology Ropar, Rupnagar, Punjab-140001, India
Email: kcjena@iitrpr.ac.in

Authors

Bhawna Rana- Department of Physics, Indian Institute of Technology Ropar, Rupnagar, Punjab-140001, India

David J. Fairhurst - Department of Physics and Mathematics, School of Science and Technology, Nottingham Trent University, Nottingham, Clifton Campus, NG11 8NS, United Kingdom

Author Contributions

All authors have given approval to the final version of the manuscript.

Notes

The authors declare no competing financial interest.

ACKNOWLEDGMENT

We are grateful to Jahur A. Mondal, Kamal P. Singh and Manoranjan Mishra for the fruitful discussions. K. C. J. sincerely acknowledges the financial support from the Indian Institute of Technology Ropar for the development of research infrastructure under central facility, SEED grants and the Science and Engineering Resaerch Board (SERB), India (CRG/2018/004975). B. R. acknowledges the British Council for Newton Bhabha fund ID: 544025790 to provide an opportunity to collaborate and carry out research at Nottingham Trent University, United Kingdom.

ABBREVIATIONS

VIS, Visible; IR, infrared; HWHM, Half width at half maxima; SFG, Sum frequency generation.

REFERENCES

(1) Li, Y.; Diddens, C.; Segers, T.; Wijshoff, H.; Versluis, M.; Lohse, D. Evaporating droplets on oil-wetted surfaces: Suppression of the coffee-stain effect. *Proc. Natl. Acad. Sci.* **2020**, *117* (29), 16756-16763.

(2) Jing, J.; Reed, J.; Huang, J.; Hu, X.; Clarke, V.; Edington, J.; Housman, D.; Anantharaman, T. S.; Huff, E. J.; Porter, B.; Shenker, A.; Wolfson, E.; Hiort, C.; Kantor, R.; Aston, C.; Schwartz, D. C. Automated high resolution optical mapping using arrayed, fluid-fixed DNA molecules. *Proc. Natl. Acad. Sci.* **1998**, *95*(14), 8046-8051.

(3) Squyres, S. W., Grotzinger, J. P., Arvidson, R. E., Bell III, J. F., Calvin, W., Christensen, P. R.; Clark, B. C.; Crisp, J. A.; Farrand, W. H.; Herkenhoff, K. E.; Johnson, J. R.; Klingelhöfer, G.; Knoll, A. H.; Mclennan, S. M.; Mcsween Jr., H. Y.; Morris, R. V.; Rice Jr., J. W.; Rieder, R.; Soderblom, L. A. In situ evidence for an ancient aqueous environment at Meridiani Planum, Mars. *Science* **2004**, *306* (5702), 1709-1714.

(4) Wang, X.; Zhang, M.; Schubert, D. W.; Liu, X. Oil-Water Separation Polypropylene Foam with Advanced Solvent-Evaporation Induced Coexistence of Microspheres and Microporous Structure. *Macromol. Rapid Commun.* **2022**, 2200177.

(5) Tao, P.; Ni, G.; Song, C.; Shang, W.; Wu, J.; Zhu, J.; Chen. G.; Deng, T. Solar-driven interfacial evaporation. *Nat. Energy* **2018**, *3*(12), 1031-1041.

(6) Brutin, D.; Sobac, B.; Loquet, B.; Sampol, J. Pattern formation in drying drops of blood. *J. of fluid Mech.* **2011**, *667*, 85-95.

(7) Rosenfeld, D.; Lohmann, U.; Raga, G. B.; O'Dowd, C. D.; Kulmala, M.; Fuzzi, S.; Reissell, A.; Andreae, M. O. Flood or drought: how do aerosols affect precipitation?. *Science*, **2008**, *321*(5894), 1309-1313.

(8) Rosenfeld, D. Suppression of rain and snow by urban and industrial air pollution. *Science* **2000**, *287*(5459), 1793-1796.

(9) Clement, A. C.; Burgman, R.; Norris, J. R. Observational and model evidence for positive low-level cloud feedback. *Science* **2009**, *325*(5939), 460-464.

(10) Moore, F. G.; Richmond, G. L. Integration or segregation: how do molecules behave at oil/water interfaces?. *Acc. Chem. Res.* **2008**, *41*(6), 739-748.

(11) Ji, N.; Ostroverkhov, V.; Tian, C. S.; Shen, Y. R. Characterization of vibrational resonances of water-vapor interfaces by phase-sensitive sum-frequency spectroscopy. *Phys. Rev. Lett.* **2008**, *100*(9), 096102.

(12) Pahlavan, A. A.; Yang, L.; Bain, C. D.; Stone, H. A. Evaporation of Binary-Mixture Liquid Droplets: The Formation of Picoliter Pancakelike Shapes. *Phys. Rev. Lett.* **2021**, *127*(2), 024501.

(13) Li, Y.; Diddens, C.; Lv, P.; Wijshoff, H.; Versluis, M.; Lohse, D. Gravitational effect in evaporating binary microdroplets. *Phys. Rev. Lett.* **2019**, *122*(11), 114501.

(14) Jaiswal, V.; Dwivedi, R. K.; Harikrishnan, A. R.; Dhar, P. Magnetohydrodynamics-and magnetosolutal-transport-mediated evaporation dynamics in paramagnetic pendant droplets under field stimulus. *Phys. Rev. E* **2018**, *98*(1), 013109.

(15) Edwards, A. M. J.; Atkinson, P. S.; Cheung, C. S.; Liang, H.; Fairhurst, D. J.; Ouali, F. F. Density-driven flows in evaporating binary liquid droplets. *Phys. Rev. Lett.* **2018**, *121*(18), 184501.

(16) Varilly, P.; Chandler, D. Water evaporation: A transition path sampling study. *J. Phys. Chem.* B **2013**, *117*(5), 1419-1428.

(17) Mason, P. E. Molecular dynamics study on the microscopic details of the evaporation of water. *J. Phys. Chem. A* **2011**, *115*(23), 6054-6058.

(18) Nagata, Y.; Usui, K.; Bonn, M. Molecular mechanism of water evaporation. *Phys. Rev. Lett.* **2015**, *115*(23), 236102.

(19) Musolino, N.; Trout, B. L. Insight into the molecular mechanism of water evaporation via the finite temperature string method. *J. Chem. Phys.* **2013**, *138*(13), 134707.

(20) Du, Q.; Superfine, R.; Freysz, E.; Shen, Y. R. Vibrational spectroscopy of water at the vapor/water interface. *Phys. Rev. Lett.* **1993**, *70*(15), 2313.

(21) Mondal, J. A.; Nihonyanagi, S.; Yamaguchi, S.; Tahara, T. Three distinct water structures at a zwitterionic lipid/water interface revealed by heterodyne-detected vibrational sum frequency generation. *J. Am. Chem. Soc.* **2012**, *134*(18), 7842-7850.

(22) Scheu, R.; Rankin, B. M.; Chen, Y.; Jena, K. C.; Ben-Amotz, D.; Roke, S. Charge asymmetry at aqueous hydrophobic interfaces and hydration shells. *Angew. Chem.* **2014**, *126*(36), 9714-9717.

(23) Chaudhary, S.; Kaur, H.; Kaur, H.; Rana, B.; Tomar, D.; Jena, K. C. Probing the Bovine Hemoglobin Adsorption Process and its Influence on Interfacial Water Structure at the Air–Water Interface. *Appl. Spectrosc.* **2021**, *75*(12), 1497-1509.

(24) Tyrode, E.; Johnson, C. M.; Kumpulainen, A.; Rutland, M. W.; Claesson, P. M. Hydration state of nonionic surfactant monolayers at the liquid/vapor interface: Structure determination by vibrational sum frequency spectroscopy. *J. Am. Chem. Soc.* **2005**, *127*(48), 16848-16859.

(25) Hofmeister, F. Zur Lehre Von Der Wirkung Der Salze. *NaunynSchmiedeberg's Arch. Pharmacol.* **1888**, 25, 1-30

(26) Chen, X.; Yang, T.; Kataoka, S.; Cremer, P. S. Specific ion effects on interfacial water structure near macromolecules. *J. Am. Chem. Soc.* **2007**, *129*(40), 12272-12279.

(27) Roy, S.; Mondal, J. A. Kosmotropic Electrolyte (Na2CO3, NaF) Perturbs the Air/Water Interface through Anion Hydration Shell without Forming a Well-Defined Electric Double Layer. *J. Phys. Chem. B* **2021**, *125*(16), 3977-3985.

(28) Jubb, A. M.; Hua, W.; Allen, H. C. Organization of water and atmospherically relevant ions and solutes: vibrational sum frequency spectroscopy at the vapor/liquid and liquid/solid interfaces. *Acc. Chem. Res.* **2012**, *45*(1), 110-119.

(29) Tian, C.; Byrnes, S. J.; Han, H. L.; Shen, Y. R. Surface propensities of atmospherically relevant ions in salt solutions revealed by phase-sensitive sum frequency vibrational spectroscopy. *J. Phys. Chem. Lett.* **2011**, *2*(15), 1946-1949.

(30) Piatkowski, L.; Zhang, Z.; Backus, E. H.; Bakker, H. J.; Bonn, M. Extreme surface propensity of halide ions in water. *Nat. Commun.* **2014**, *5*(1), 1-7.

(31) O'Brien, J. T.; Prell, J. S.; Bush, M. F.; Williams, E. R. Sulfate ion patterns water at long distance. *J. Am. Chem. Soc.***2010**, *132*(24), 8248-8249.

(32) Verma, G.; Singh, K. P. Time-resolved interference unveils nanoscale surface dynamics in evaporating sessile droplet. *Appl. Phys. Lett.* **2014**, *104*(24), 244106.

(33) Tomar, D.; Rana, B.; Jena, K. C. The structure of water–DMF binary mixtures probed by linear and nonlinear vibrational spectroscopy. *J. Chem. Phys.* **2020**, *152*(11), 114707.

(34) Kaur, H.; Chaudhary, S.; Kaur, H.; Chaudhary, M.; Jena, K. C. Hydrolysis and Condensation of Tetraethyl Orthosilicate at the Air–Aqueous Interface: Implications for Silica Nanoparticle Formation. *ACS Appl. Nano Mater.* **2021**, *5*(1), 411-422

(35) Jena, K. C.; Covert, P. A.; Hore, D. K. The effect of salt on the water structure at a charged solid surface: Differentiating second-and third-order nonlinear contributions. J. Phys. Chem. Lett. **2011**, *2*(9), 1056-1061.

(36) Azam, M. S.; Cai, C.; Gibbs, J. M.; Tyrode, E.; Hore, D. K. Silica surface charge enhancement at elevated temperatures revealed by interfacial water signals. *J. Am. Chem. Soc.* **2020**, *142*(2), 669-673.

(37) Troiano, J. M.; McGeachy, A. C.; Olenick, L. L.; Fang, D.; Liang, D.; Hong, J.; Kuech T. R.; Caudill E. R.; Pedersen J. A.; Cui Q.; Geiger, F. M. Quantifying the electrostatics of polycation–lipid bilayer interactions. *J. Am. Chem. Soc.* **2017**, *139*(16), 5808-5816.

(38) Rogers, M. M.; Neal, J. F.; Saha, A.; Algarni, A. S.; Hill, T. C., Allen, H. C. The Ocean's Elevator: Evolution of the Air–Seawater Interface during a Small-Scale Algal Bloom. *ACS Earth Space Chem.* **2020**, *4*(12), 2347-2357.

(39) Strazdaite, S.; Versluis, J.; Backus, E. H.; Bakker, H. J. Enhanced ordering of water at hydrophobic surfaces. *J. Chem. Phys.* **2014**, *140*(5), 054711.

(40) Dalchand, N.; Dogangun, M.; Ohno, P. E.; Ma, E.; Martinson, A. B.; Geiger, F. M. Perturbation of hydrogen-bonding networks over supported lipid bilayers by poly (allylamine hydrochloride). *J. Phys. Chem. B* **2019**, *123*(19), 4251-4257.

(41) Smolentsev, N.; Smit, W. J.; Bakker, H. J.; Roke, S. The interfacial structure of water droplets in a hydrophobic liquid. Nat. Commun. **2017**, *8*(1), 1-6.

(42) Ishiyama, T.; Morita, A. Nuclear quantum effect on the χ (2) band shape of vibrational sum frequency generation spectra of normal and deuterated water surfaces. *J. Phys. Chem. Lett.* **2019**, *10*(17), 5070-5075.

(43) Wei, X.; Shen, Y. R. Motional effect in surface sum-frequency vibrational spectroscopy *Phys. Rev. Lett.* **2001**, *86*(21), 4799.

(44) Gan, W.; Wu, D.; Zhang, Z.; Feng, R. R.; Wang, H. F. Polarization and experimental configuration analyses of sum frequency generation vibrational spectra, structure, and orientational motion of the air/water interface. *J. Chem. Phys.* **2006**, *124*(11), 114705.

(45) Sun, S.; Tang, F.; Imoto, S.; Moberg, D. R.; Ohto, T.; Paesani, F.; Bonn. M.; Backus, E. H. G.; Nagata, Y. Orientational distribution of free OH groups of interfacial water is exponential. *Phys. Rev. Lett.* **2018**, *121*(24), 246101.

(46) Boily, J. F.; Fu, L.; Tuladhar, A.; Lu, Z.; Legg, B. A.; Wang, Z. M.; Wang, H. Hydrogen bonding and molecular orientations across thin water films on sapphire. *J. Colloid Interface Sci.***2019**, *555*, 810-817.

(47) Feng, R. R.; Guo, Y.; Wang, H. F. Reorientation of the "free OH" group in the top-most layer of air/water interface of sodium fluoride aqueous solution probed with sum-frequency generation vibrational spectroscopy. *J. Chem. Phys.***2014**, *141*(18), 18C507.

(48) Luzar, A.; Chandler, D. Hydrogen-bond kinetics in liquid water. *Nature* **1996**, *379*(6560), 55-57.

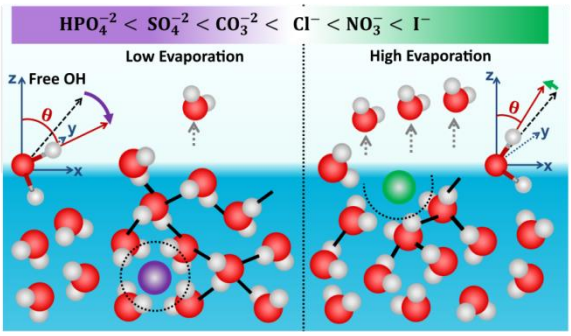
$HPO_4^{-2} < SO_4^{-2} < CO_3^{-2} < Cl^- < NO_3^- < I^-$
Low Evaporation
High Evaporation
Free OH
z
θ
y
x